Australian Journal of Science and Technology
ISSN Number (2208-6404)
Volume 5; Issue 4; December 2021

Original Article

Oxidation of a 4 wt.% Hf–containing nickel–based alloy at temperatures ranging from 1100°C to 1250°C in air

Patrice Berthod[1,2]*, Dame Assane Kane[2], Lionel Aranda[1]

[1]Department of Chemistry and Physics of Solids and Surfaces, Institut Jean Lamour (UMR CNRS 7198), Université de Lorraine, Nancy, France, [2]Department of Chemistry, Faculté des Sciences et Technologies, Université de Lorraine, Nancy, France

ABSTRACT

The needs of metallic alloys able to work at elevated temperatures in severe conditions of applied mechanical stresses and chemical aggressivity of the environment is increasing more and more. For service temperatures equal to, or higher than, 1100°C, new superalloys must developed because of the loss in strengthening particles known by γ/γ' single crystals at so high temperatures, or the difficult availability of Oxide Dispersion Strengthened superalloys for geometrically complex hot components. Traditional metallurgical solutions are still a source of new superalloys development if innovative phases can be obtained in the microstructures. Carbides with complex constitutions represent a possible long-lasting strengthening system in cast polycrystalline alloys which are the most adapted alloys to produce coarse–grained complex pieces. In this work this is the (Hf, Ta) C strengthening system in a chromia–forming austenitic nickel–based matrix which was under interest. Interesting creep resistance at high temperature (e.g. 1100°C) were recently observed. In order to evaluate the chemical resistance at the same temperature for this type of materials, the same alloy was here exposed to synthetic air at 1100°C during 50 h in a thermobalance, followed by the post–mortem characterization of the oxidized states. To explore its oxidation resistance to more elevated temperatures this test was carried out 2 times more, at 1200°C and 1250°C. For these three temperatures this alloy well behaved in hot oxidation was good: chromia–forming behavior, rather slow oxidation kinetics and acceptable resistance against oxide scale spallation when cooling.

Keywords: Nickel–chromium alloy, high Hf content, high temperature oxidation, thermogravimetry, metallographic characterization

Submitted: 18-02-2021, **Accepted:** 30-08-2021, **Published:** 30-12-2021

GRAPHICAL ABSTRACT

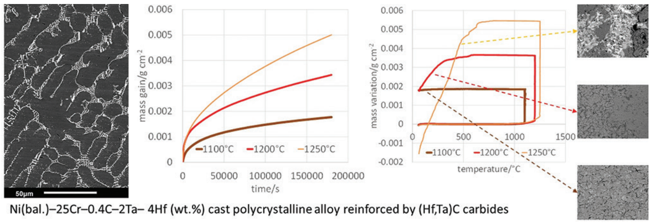

Ni(bal.)–25Cr–0.4C–2Ta– 4Hf (wt.%) cast polycrystalline alloy reinforced by (Hf,Ta)C carbides

INTRODUCTION

Superalloys, metallic alloys for applications at elevated temperatures in conditions of severe mechanical and chemical solicitations, are based on more or less refractory metals (nickel, cobalt, and niobium) and often contain also very particular elements in small quantities for enhancing some properties. This is the case of hafnium. Due to its special behavior in situation of high-temperature oxidation,[1,2] hafnium is often added in the chemical compositions of high-temperature metallic materials based on various metals: classical Ni–based and Co–based superalloys,[3] but also Nb–based refractory alloys[4-7] or nickel aluminides.[8,9] New categories of alloys may also contain Hf, such as high entropy alloys,[10-12] shape memory alloys,[13-16] metallic coatings,[17,18] and ceramics.[19,20]

Address for correspondence: Patrice Berthod, Department of Chemistry and Physics of Solids and Surfaces, Institut Jean Lamour (UMR CNRS 7198), Université de Lorraine, Nancy, France. E-mail: patrice.berthod@univ-lorraine.fr

Some alloys can also exploit the high carbide–former power of hafnium. In presence of carbon Hf may form HfC monocarbides. A rather long time ago this ability was used in metallic alloys based on heavy refractory metals (e.g. molybdenum–based, tungsten–based). More recently this was successfully exploited in superalloys based on more common metals, such as cobalt.[21] In the present work this is in a nickel–chromium cast alloy that Hf will be introduced to form MC carbides for mechanical reinforcement purpose, but not alone: with another MC–former element, tantalum. The microstructure of this alloy highly alloyed with hafnium in its as–cast state will be observed by electron microscopy and its refractoriness explored by high-temperature scanning calorimetry. In a 2nd time, this alloy rich in an element known for its particular hot oxidation behavior, will be exposed to air at three different levels of high temperature, to explore its chemical resistance in oxidant gaseous environment.

MATERIALS AND METHODS

Elaboration of the Alloy

The alloy designed and elaborated for these investigations was a Ni(bal.)–25Cr–0.4C–2Ta–4Hf one (all contents in wt.%). Pure elements (Ni, Cr, C, Hf, and Ta; purity of 99.9 wt.% and more) were melted together in a CELES (France) high-frequency induction furnace in an inert atmosphere composed of pure argon (pressure: half of 1 atm). The values of the main operating parameters were: frequency of about 110 kiloHertz, voltage of 5 kilo Volts, temperature and time of stay at in the liquid state of about 1600°C and 5 min. After complete cooling, an ovoidal ingot weighing close to 40 g was obtained. It was cut in several parts, with shapes, sizes, and surface state depending on their destinations.

Microstructure Investigations

A part (globally cubic, with approximate dimensions 10 × 10 × 10 mm^3) was embedded in resin, ground and polished until a mirror-like state was obtained. The microstructure and chemical composition were controlled using a JEOL (Japan) JSM6010-LA scanning electron microscope (SEM) in backscattered electrons mode (BSE), an its energy dispersion spectrometer (EDS), respectively.

Determination of the Temperature of Melting Start

Prior to exposing the alloy to temperatures as high as the ones envisaged for the oxidation tests, the refractoriness of the alloy was measured to check whether the alloy will remain totally solid during these tests. This verification was done by re–melting a 2.5 × 2.5 × 8 mm^3 part of the alloy by applying a heating at +5K min^{-1} up to almost 1500°C, using a SETARAM (France) TG–ATD apparatus, and by recording the heat exchanges between the sample and the apparatus.

Oxidation Runs and Exploitation

Three samples, with 10 × 10 × 3 mm^3 as approximate dimensions, ground using 1200–grit SiC papers. Their edges and corners were carefully smoothed to avoid any local catastrophic oxidation. A sample was exposed at 1100°C, another one at 1200°C and the third one at 1250°C, in a SETARAM (France) TGA92 thermobalance continuously crossed by a 1.5 L/h flow of synthetic air, during 50 h in all cases. The applied heating and cooling rates were respectively +20K min^{-1} and -5K min^{-1}.

Characterization of the Oxidized States

The external morphology oxides formed over the samples were first characterized by X–ray diffraction (XRD) using a BRUKER (USA) D8 Advance diffractometer. Thereafter, they were observed with the SEM in secondary electrons mode after preliminary gold deposition by cathodic evaporation. This was followed by the electrolytic deposition of nickel all around the oxidized samples and by their cutting in order to prepare cross–sections for the observation of the external and internal oxides as well as of the subsurface degradation induced by hot oxidation.

RESULTS AND DISCUSSION

Initial Characteristics of the Alloys

The mix of pure elements, weighing about 40 g, was successfully melted. The cutting of the obtained ovoid ingot to obtain all the parts necessary to the wished analyses and tests did not reveal not melted parts of the initial pure elements. The control of the alloy's chemical composition by EDS allowed verifying that the wished composition was really obtained. The initial microstructure of the alloy is illustrated by a SEM/BSE micrograph shown in Figure 1 in which both phases of this double–phased alloy are presented (austenitic Ni matrix and interdendritic carbides of a single type: MC). This is the same type of microstructure as the alloy which recently demonstrated high potential of mechanical resistance at 1100°C. The DSC run showed that the melting start temperature was several tens degrees above the maximal temperature of oxidation test (1250°C).

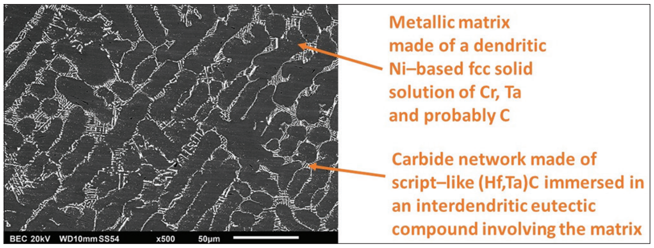

Figure 1: Microstructure of the studied alloy as produced by casting (scanning electron microscope/back scattered electrons mode)

Oxidation Kinetics

The three mass variation files recorded during the thermogravimetry tests at 1100, 1200 and 1250°C were exploited on their three distinct parts: heating, isothermal stage, cooling.

Heating

The mass variations during the heating phases of the three tests, preliminarily corrected (from the air buoyancy variation due to the temperature change), are plotted together in Figure 2. There is a lack of reproducibility since the mass gain by oxidation for the curve leading to the 1100°C isothermal stage temperature, became detectable a little later than the mass gains for the curves leading to 1200 and 1250°C: about 825°C for the former and just a little <800°C for the two latter. This is not dependent on the thermal cycle itself (the three cycles were identical to one another over this heating part up to 1100°C) but this can be attributed to possible small differences of sample cutting and surface initialization despite that the sample preparation was carried out in exactly the same conditions.

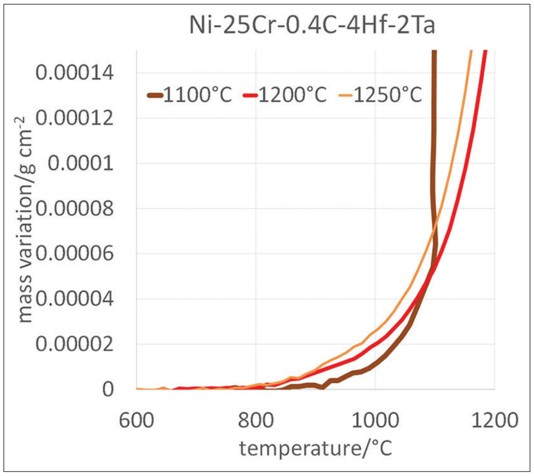

Figure 2: Start of oxidation during heating as detected by mass gain after correction from air buoyancy variation

Isothermal stage

The oxidation during the last part of heating is rather important to know since it gives information about the reactivity of the alloy–the lower the oxidation start temperature the more reactive the alloy–and on the contribution of the heating phase in the total quantity of formed oxides, this is the mass gain/quantity of oxides achieved during the isothermal stage which is predominant. The mass gain curves during the isothermal stage are plotted together in Figure 3. Whatever the temperature of the isothermal stage the mass gain kinetic is parabolic, this suggesting an oxidation rate governed by the resistance of a continuous oxide barrier opposed to the diffusion of the species involved in the oxidation reaction. The total mass gains measured at the end of the 50 h of isothermal exposure to the airflow are about 1.8 mg cm^{-2} for the 1100°C–curve, 3.4 mg cm^{-2} for the 1200°C–curve, and 5 mg cm^{-2} for the 1250°C–curve. This corresponds to the following values of the parabolic constant Kp present in the Wagner's law $\Delta m/S\,(t) = (2\,Kp_T \times t)^{1/2}$: $Kp_{1100°C} = 9 \times 10^{-6}$ mg^2 cm^{-4} s^{-1}, $Kp_{1200°C} = 32 \times 10^{-6}$ mg^2 cm^{-4} s^{-1} and $Kp_{1250°C} = 69 \times 10^{-6}$ mg^2 cm^{-4} s^{-1}. These values globally correspond to the Kp values of chromia – forming alloys for the same temperatures before being corrected from chromia–volatilization. This correction consists in taking into account the continuous mass loss induced by the re–oxidation of chromia (Cr_2O_3) in volatile oxides CrO_3. (phenomenon starting at 1000°C and becoming more and more important for temperatures higher and higher. It is possible to take this phenomenon into account by adding to the mass gain isothermally achieved, an approximate value of the mass lost consequently to the emission of gaseous CrO_3: this one can be estimated by multiplying a known value of the volatilization constant Kv by the isothermal stage duration. Kv was earlier determined by studying a really chromia–forming model alloy (Ni–30 wt.%Cr):[22] the values of Kv at 1000, 1100 and 1200°C in (20% O_2–80% N_2, 1 atm.)–synthetic air were, respectively, about 90×10^{-7} mg/cm^2, 160×10^{-7} mg/cm^2 and 200×10^{-7} mg/cm^2 (for 1250°C: Arrhenian interpolation between 1200°C and 1300°C). After the corresponding additions of (chromia volatilization)–induced mass losses (1.6, 2.9 and 3.6 mg cm^{-2}), the theoretical isothermal mass gains become 3.4 mg cm^{-2} (1100°C), 6.3 mg cm^{-2} (1200°C) and 8.6 mg cm^{-2} (1250°C) and the real Kp: 32×10^{-6} mg^2 cm^{-4} s^{-1}, 110×10^{-6} mg^2 cm^{-4} s^{-1} and 205×10^{-6} mg^2 cm^{-4} s^{-1} (values now not underestimated because chromia volatilization taken into account). These values are higher than (but not very far from) the real Kp values earlier obtained for the Ni–30wt.%Cr alloy (e.g. about 25×10^{-6} mg^2 cm^{-4} s^{-1} for 1100°C or 70×10^{-6} mg^2 cm^{-4} s^{-1} for 1200°C) for which chromia was really the single oxide to form. This suggests that, in the present case, other oxides formed in addition to chromia.

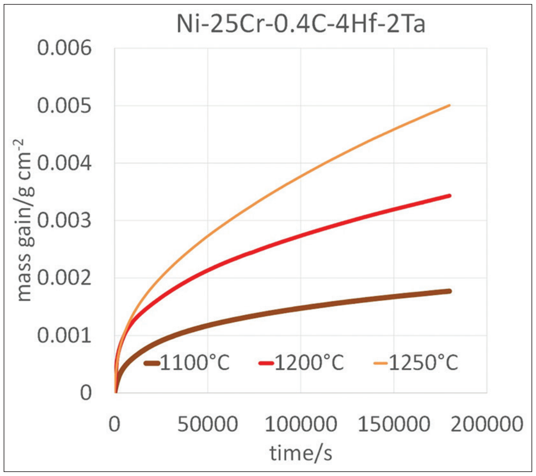

Figure 3: Progress of mass gain during isothermal oxidation at each of the three temperatures of interest

Cooling

The third and last part of interest in the three mass variation curves is the one corresponding to cooling. If the formed oxide (mainly the one formed during the isothermal stage) remains on the samples until this one is again at ambient temperature, the corresponding mass variation curve remains almost horizontal from the isothermal stage temperature and the ambient temperature, in a (mass versus time) representation as adopted in Figures 2 and 4. In Figure 4 this is the case of the 1100°C–curve. In contrast, when the external oxides failed under the compressive stresses induced by the difference of thermal contraction between oxide scale and alloy, they can fall part by part. For the sample, this results in an irregular decrease in mass progressing during all the cooling from the temperature at which the phenomenon started, down to ambient temperature generally. This obviously occurred for the oxidized sample cooling from the stage at 1200°C (start near 600°C) and for the oxidized sample cooling from the stage at 1250°C (start at about 750°C). The sample oxidized during 50 h at 1100°C is expected to have kept all its external chromia scale while parts of chromia will be probably missing over the sample oxidized at 1200°C (mass gain of only 1.8 mg cm^{-2} at the end of the whole thermal cycle against 3.6 mg cm^{-2} just before the cooling start). The mass balance sheet is even severely negative for the sample oxidized at 1250°C and back to ambient temperature (–1.5 mg cm^{-2}): it has surely lost all the external oxide formed all along the whole thermal cycle.

Post–mortem Characterization

XRD results

After removing the oxidized samples from the thermobalance, they were subjected to XRD. The three obtained diffractograms, all presented together in Figure 5, reveal that there are two main oxides on the surfaces of the three oxidized samples: chromia (Cr_2O_3) and Cr (Hf, Ta) O_4. Cr_2O_3 is predominant at the surface of the sample oxidized at 1100°C while this is the Cr (Hf, Ta) O_4 oxide which predominates over the sample oxidized at 1250°C.

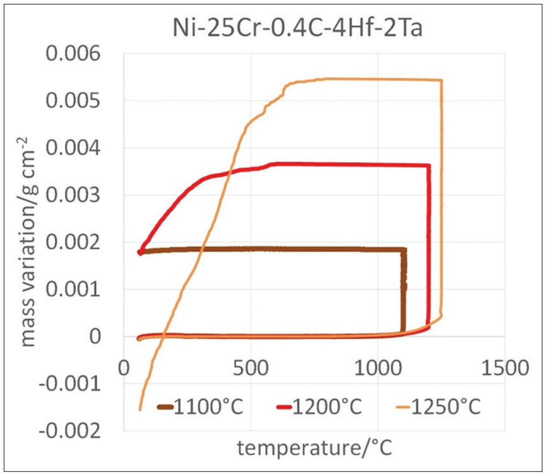

Figure 4: Mass losses during cooling due to oxide scale spallation

Samples' external aspect

The observation with the naked eyelet think first that the external aspect of the three oxidized samples were different. After cathodic pulverization of an extra–thin gold layer, the surfaces of the oxidized samples were observed with the SEM. Some micrographs taken in SE mode are presented in Figure 6, and other ones taken in BSE mode, shown in Figure 7, give some qualitative information about the average atomic number of the seen phases. With considering the XRD results in parallel, it clearly appears that the sample oxidized at 1100°C is uniformly covered by a fine–grained scale of chromia. This is also the case of the sample oxidized at 1200°C but some flat zones suggest that the external part of chromia was lost by shear rupture and spallation. However, the sample is still almost wholly covered by chromia (dark

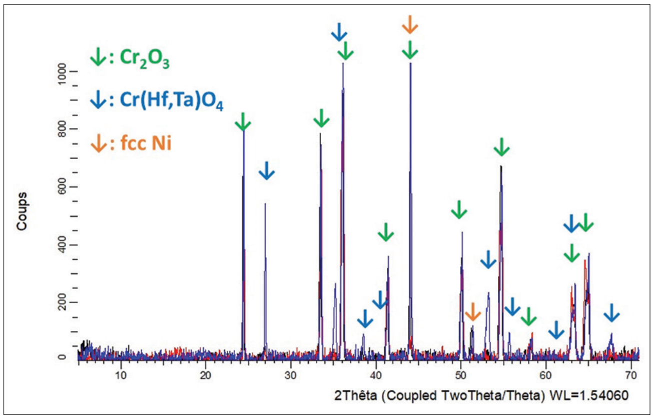

Figure 5: X-ray diffractograms of the sample's surface oxidized at 1100°C (black spectrum), 1200°C (red spectrum), and 1250°C (blue spectrum)

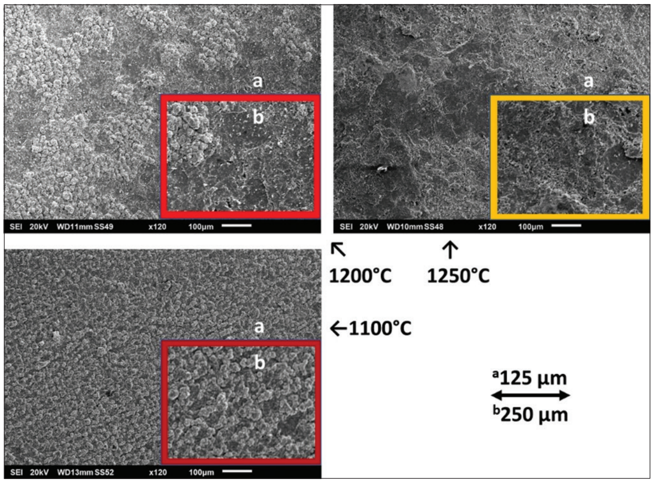

Figure 6: Oxidized states of the samples' surfaces (scanning electron microscope/secondary electrons)

gray everywhere in BSE mode), thick (grained zones), or thin (flat unruffled zones). Some areas of the external surface of the sample oxidized at 1250°C have obviously lost all the local thickness of chromia, allowing the observation of subjacent oxides containing Hf and Ta (bright) and even the alloy itself (pale gray).

Cross–sectional aspect

After the XRD and the surface observations, a nickel shell was electrolytically deposited all around the oxidized samples by cathodically polarizing it in a warm (50°C) Ni^{2+}–rich Watt's solution. This allowed cutting the samples in two halves with the limitation of loss of the external oxides. The obtained–cross sections allowed SEM/BSE examinations, EDS spot analyses, and X–maps acquisitions. Three SEM/BSE micrographs were taken per sample for three different magnifications. They are presented in Figures 8-10 for the samples oxidized at 1100°C, 1200°C, and 1250°C, respectively. The oxidation products, identified by spot EDS analysis (example in the high magnification micrograph in [Figure 11]) and elemental X–map [Figure 12], are the same in the three cases: chromia (dark gray external scale) and Cr (Hf, Ta) O_4 (interfacial and internal bright oxide) The differences between the results of the three oxidation temperatures are the following ones. The higher the oxidation temperature, the greater the quantity of Cr (Hf, Ta) O_4 and the denser the presence of this oxide at the alloy/chromia interface. Concerning the subsurface, the higher the oxidation temperature, the deeper the zone of the disappearance of the interdendritic carbides and of reprecipitation of secondary MC carbides.

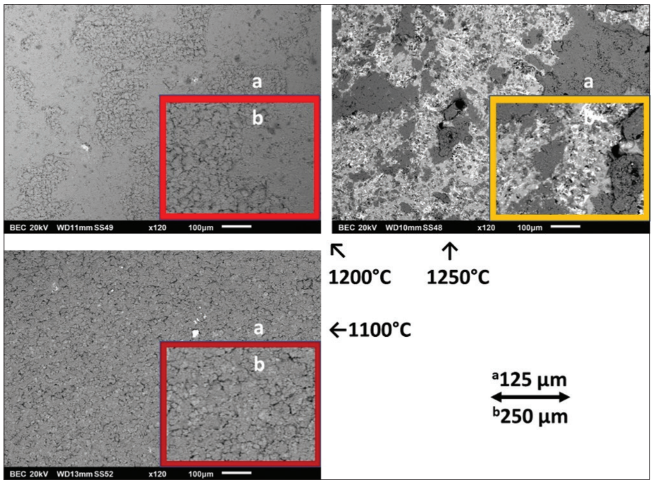

Figure 7: Oxidized states of the samples' surfaces (scanning electron microscope/back scattered electrons mode)

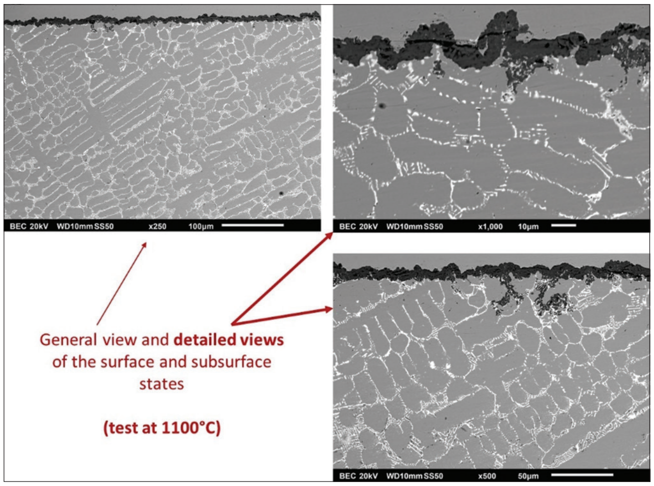

Figure 8: General (left) and detailed (right) illustrations of the oxidized state after 50 h at 1100°C (oxidized surface and oxidation–induced deterioration in subsurface)

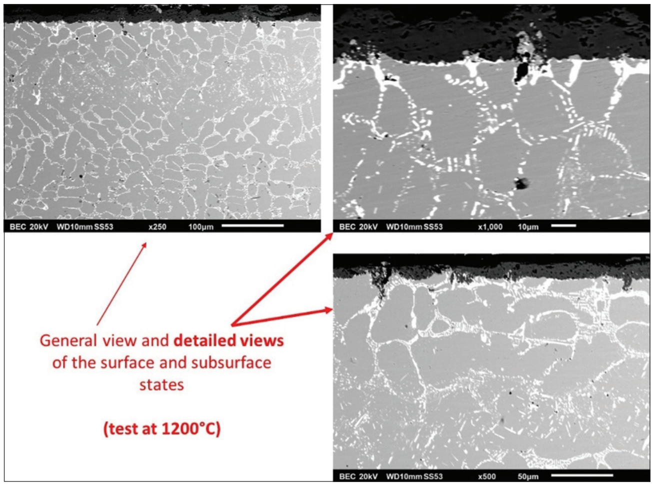

Figure 9: General (left) and detailed (right) illustrations of the oxidized state after 50 h at 1200°C (oxidized surface and oxidation–induced deterioration in subsurface)

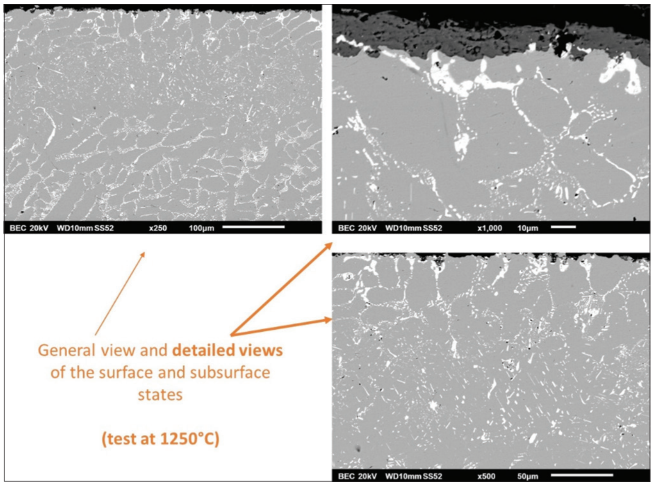

Figure 10: General (left) and detailed (right) illustrations of the oxidized state after 50 h at 1250°C (oxidized surface and oxidation–induced deterioration in subsurface)

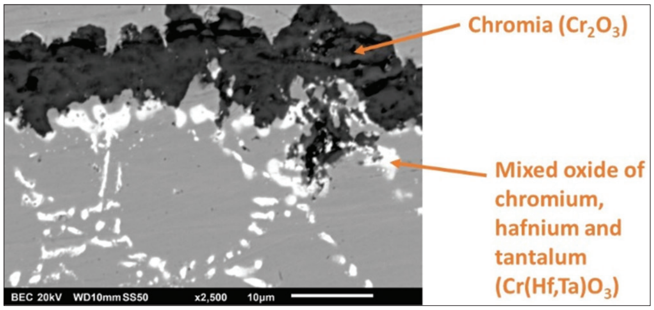

Figure 11: Identification of the formed oxides by high magnification scanning electron microscope/backscattered electrons mode imaging (here the alloy oxidized at 1100°C and observed at ×2500)

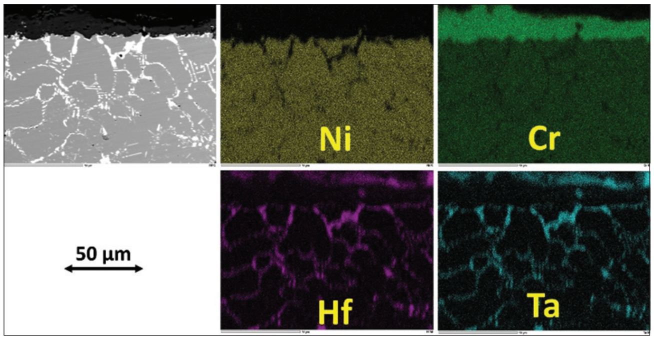

Figure 12: Scanning electron microscope/energy dispersion spectrometer elemental X–maps illustrating the oxidized state of the alloy after 50 h at 1100°C

Chemical changes in subsurface

The parabolic and rather slow mass gain kinetic still existing at the end of the isothermal stage demonstrates and the resistance of the alloy to oxidation by dry air is very satisfactory, even at the highest temperature. However, these first 50 h of oxidation have changed the subsurface in the way described just before concerning the local microstructure. The damage exists also at the chemical composition level and knowing the chemical changes in subsurface may allow anticipate about the next behavior after the 50 h. For this reason, concentration profiles were acquired inwards from the outermost surface, a least across the whole depth where microstructure changes were noted. These concentration profiles are presented in Figure 13, by one profile peroxidized sample. These ones are more or less regular, this depending on the meeting of internal oxides or of carbides by the electron beam. Globally one can observe that the subsurface is depleted in chromium and tantalum. The lowest contents in Cr and Ta are located in the extreme surface of the alloy. Five EDS spot analyses were carried out in several places very close to the extreme surface and the results allowed obtaining the average values and standard deviations which are graphically presented in Figure 14, as points and their accompanying error bars, respectively. Differences were found among the three oxidized samples as well as between these three oxidized states and the as–cast matrix one (which can play the role of reference state since the subsurfaces are

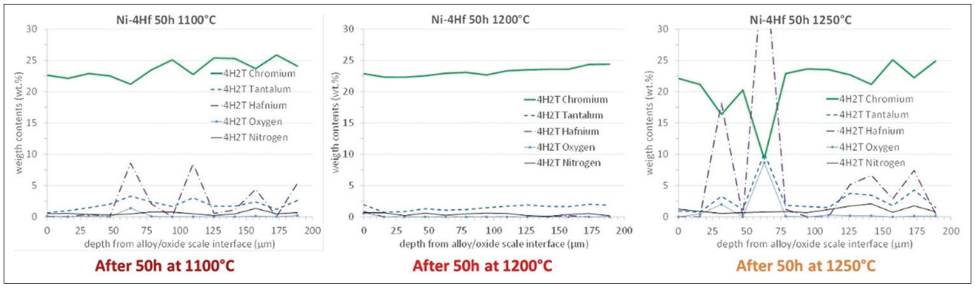

Figure 13: Inwards concentration profiles in the subsurface acquired from the extreme surface in the samples oxidized at 1100°C (left), 1200°C (middle), and 1250°C (right)

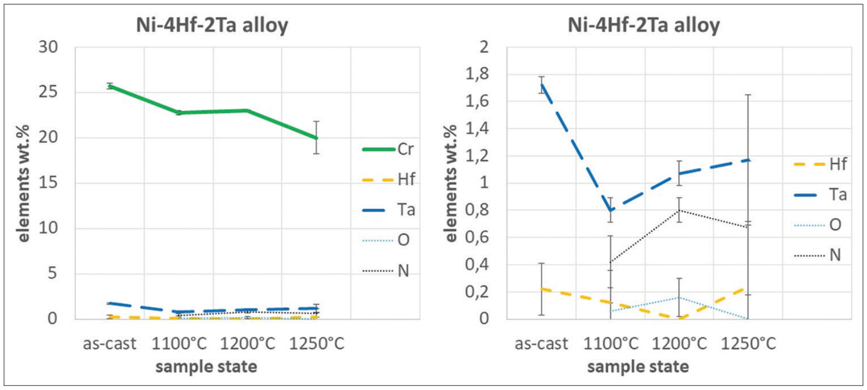

Figure 14: Composition of the extreme surface of the 50 h–oxidized alloy in chromium (left) and in Hf and Ta (right) versus the oxidation temperature

themselves free of carbides). It is clear that tantalum is present in extreme surface of the oxidized states with much lower contents than the initial ones. This is due to the formation of mixed oxides rich in tantalum. However, the main observation concerns chromium which has decreased in the outer part subsurface consequently–again to the formation of the mix oxide–but principally to the growth of a continuous thick external chromia scale. After 50 h of oxidation, the higher the isothermal stage temperature, the lower the chromium content in extreme surface. After oxidation at 1250°C for 50 h the outermost chromium content is now of about 20w wt.%, as is to say close to the Cr level usually considered as critical for the sustainability of the chromia–forming behavior for nickel-based alloys. One can guess that during 50 h more, the alloy may encounter local starts of generalized oxidation here and there. This may be worse in the case of thermal cycling since, as this was noticed here, the alloy may know oxide spallation after 50 h of oxidation at this temperature.

CONCLUSION

The Ni–based 25wt.% Cr–containing (Hf, Ta) C–strengthened alloy object of this high-temperature oxidation work is easy to produce by casting but refractory enough to be used as structural parts in the hottest zones of industrial machines or power generation and aeronautical turbines. It was seen in another work that its particular MC carbides allow it to oppose significant resistance against creep, at least at 1100°C. In the present study, it appeared that the behavior of this alloy in oxidation at this same temperature is very good: parabolic mass gain, low oxidation rate, and very good resistance against oxide spallation. Apart from the lack of oxide stability at cooling after oxidation at 1200 and 1250°C, higher temperatures, the overall oxidation behavior at these higher temperatures are still satisfactory for the same 50 h duration. However, the inescapable impoverishment in chromium in the outermost subsurface may lead the alloy losing its chromia–forming behavior sooner or later. This is not surprising but it is possible that this may take place shortly in the case of 1250°C, maybe even before 100 h. In addition, real uses necessarily involve variations in temperature and the lack of resistance against oxide spallation after oxidation at this highest temperature will surely precipitate the start of catastrophic oxidation. Hence, despite the very honorable oxidation behavior of this alloy, a protective coating should be envisaged for uses at so high temperature.

ACKNOWLEDGMENTS

The authors wish thanking the X-gamma competence center of the Jean Lamour Institut for having authorized the authors using the XRD.

CONFLICTS OF INTEREST

The authors declare that they have no conflicts of interest.

REFERENCES

1. Kofstad P. High Temperature Corrosion. United Kingdom: Elsevier; 1988.
2. Cao XZ, He J, Chen H, Zhou B, Liu L, Guo H. The formation mechanisms of HfO_2 located in different positions of oxide scales on Ni-Al alloys. Corr Sci 2020;167:108481.
3. Sims CT, Hagel WC. The Superalloys-vital High Temperature Gas Turbine Materials for Aerospace and Industrial Power. United States: John Wiley & Sons; 1972.
4. Grammenos I, Tsakiropoulos P. Study of the role of Mo and Ta additions in the microstructure of Nb-18Si-5Hf silicide based alloy. Intermetallics 2010;18:1524-30.
5. Sha JB, Liu J, Zhou C. Effect of Cr additions on toughness, strength, and oxidation resistance of a Nb-4Si-20Ti-6Hf alloy at room and/or righ temperatures. Metall Mater Trans 2011;42:1534-43.
6. Su LF, Jia L, Jiang K, Zhang H. The oxidation behavior of high Cr and Al containing Nb-Si-Ti-Hf-Al-Cr alloys at 1200 and 1250°C. Int J Refract Hard Met 2017;69:131-7.
7. Dhole A, Bhattacharya A, Gupta RK, Gokhale AA, Samajdar I. The role of the metal-oxide Interface's terminating layer on the selective cold cracking of a commercial Niobium-Hafnium-Titanium (C-103) alloy. J Alloys Compds 2020;856:157427.
8. He J, Zhang Z, Peng H, Gong S, Guo H. The role of Dy and Hf doping on oxidation behavior of two-phase (γ'+β) Ni-Al alloys. Corros Sci 2015;98:699-707.
9. Han BH, Ma Y, Peng H, Zheng L, Guo H. Effect of Mo, Ta, and Re on high-temperature oxidation behavior of minor Hf doped β-NiAl alloy. Corros Sci 2016;102:222-32.
10. Yang XX, Sha JB, Zhang H. Property responses in Nb-Si-Hf-Ti-Al-W-B-Cr alloys for high-temperature applications. Mater Sci Forum 2010;654-656:468-71.
11. Wu WQ, Ni S, Liu Y, Song M. Effects of cold rolling and subsequent annealing on the microstructure of a HfNbTaTiZr high-entropy alloy. J Mater Res 2016;31:3815-23.
12. Lu JC, Chen Y, Zhang H, Li L, Fu L, Zhao X, *et al*. Effect of Al content on the oxidation behavior of Y/Hf-doped AlCoCrFeNi high-entropy alloy. Corros Sci 2020;170:108691.
13. Vermaut P, Chastiaing K, Ochin P, Segui C. Effect of Cu additions in Ni49.8Ti40.2Hf10 shape memory alloys. Arch Metall Mater 2004;49:869-79.
14. Suresh KS, Kim DI, Bhaumik SK, Suwas S. Evolution of microstructure and texture in Ni49.4Ti38.6Hf12 shape memory alloy during hot rolling. Intermetallics 2013;42:1-8.
15. Kim KM, Yeom JT, Lee HS, Yoon SY, Kim JH. High temperature oxidation behavior of Ti-Ni-Hf shape memory alloy. Thermochim Acta 2014;583:1-7.
16. Kim JH, Kim KM, Yeom JT, Young S. Effect of yttrium on martensite-austenite phase transformation temperatures and high temperature oxidation kinetics of Ti-Ni-Hf high-temperature shape memory alloys. Met Mater Int 2016;22:204-8.
17. Soboyejo WO, Mensah PF, Diwan R, Crowe J, Akwaboa S. High-temperature oxidation interfacial growth kinetics in YSZ thermal barrier coatings with bond coatings of Ni-Co-Cr-Al-Y

with 0.25% Hf. Mater Sci Eng 2011;A528:2223-30.

18. Zhong JY, Mu RD, He LM. High temperature oxidation behaviour of plasma carburised Ni based single crystal superalloy with NiCoCrAlYHf high temperature oxidation protective coatings. Mater Res Innov 2014;18:1115-20.
19. Zeman P, Zuzjaková Š, Mareš P, Čerstvý R, Zhang M, Jiang J, *et al*. Superior high-temperature oxidation resistance of magnetron sputtered Hf-B-Si-C-N film. Ceram Int 2016;42:4853-9.
20. Zhang MH, Jiang J. Study of the high-temperature oxidation resistance mechanism of magnetron sputtered Hf7B23Si17C4N45 film. J Vac Sci Technol A 2018;36:021505.
21. Berthod P. High temperature properties of several chromium-containing Co-based alloys reinforced by different types of MC carbides (M=Ta, Nb, Hf and/or Zr). J Alloys Compd 2009;481:746-54.
22. Berthod P. Kinetics of high temperature oxidation and chromia volatilization for a binary Ni-Cr alloy. Oxid Met 2005;64:235-52.